Inorganic Chemistry

Article

pubs.acs.org/IC

Structural Phase Transitions of a Layered Organic–Inorganic Hybrid Compound: Tetra(cyclopentylammonium) Decachlorotricadmate(II), $[C_5H_9NH_3]_4Cd_3Cl_{10}$

Wei-Qiang Liao,[†] Guang-Quan Mei,*[,‡] Heng-Yun Ye,[†] Ying-Xuan Mei,[‡] and Yi Zhang*[,†]

[†]Ordered Matter Science Research Center, Southeast University, Nanjing 211189, PR China

[‡]Key Laboratory of Jiangxi University for Applied Chemistry and Chemical Biology, Yichun University, Yichun 336000, China

Supporting Information

ABSTRACT: A layered organic–inorganic hybrid compound, tetra(cyclopentylammonium) decachlorotricadmate(II) (**1**), in which the two-dimensional $[Cd_3Cl_{10}]^{4-}_n$ networks built up from three face-sharing $CdCl_6$ octahedra are separated by cyclopentylammonium cation bilayers, has been discovered as a new phase transition material. It undergoes two successive structural phase transitions, at 197.3 and 321.6 K, which were confirmed by differential scanning calorimetry measurements, variable-temperature structural analyses, and dielectric measurements. The crystal structures of **1** determined at 93, 298, and 343 K are solved in $P2_12_12_1$, *Pbca*, and *Cmca*, respectively. A precise analysis of the structural differences between these three structures reveals that the origin of the phase transition at 197.3 K is ascribed to the order–disorder transition of the cyclopentylammonium cations, while the phase transition at 321.6 K originates from the distortion of the two-dimensional $[Cd_3Cl_{10}]^{4-}_n$ network.

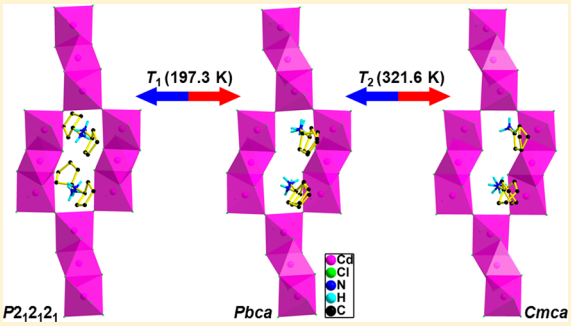

INTRODUCTION

Phase transition materials have attracted more and more attention owing to their potential applications in data storage, signal processing, sensing, switchable dielectric devices, etc.[1,2] Various approaches have been developed to prepare the phase transition materials. Among them, the synthesis of organic–inorganic hybrid compounds, which are able to combine desirable characteristics from both types of constituents, is one of the most effective methods.[3,4] In particular, the layered organic–inorganic hybrids are extensively investigated in view of their interesting structural phase transitions.[5] Earlier studies have shown that the main structural features of these layered compounds are that the inorganic layers alternate with organic bilayers or monolayers and there are hydrogen-bonding interactions between the organic and inorganic components.[6] Freezing and reorientation of the organic cations and deformation of the anionic framework were shown to easily induce the phase transitions.[7,8] Therefore, the layered organic–inorganic hybrid compounds are excellent candidates to show phase transition behaviors. Notable examples of such hybrids are compounds with the general formula $[(R\text{-}NH_3)_2MX_4]$, (where R = organic ammonium cation, M = divalent metal ion, and X = halogen), which consist of a two-dimensional network of corner-sharing MX_6 octahedra and are widely studied for their phase transition properties.[5−8] For instance, $[(C_3H_7NH_3)_2MCl_4]$ (M = Cu, Cd, and Mn) undergo structural phase transitions associated with the motion of the rigid propylammonium cation.[9] However, layered hybrids with two-dimensional $[M_3X_{10}]^{4-}_n$ networks of three face-sharing MX_6 octahedra are very sparse.[10]

In the course of exploring new phase transition materials,[11−14] we discovered that the reaction of $CdCl_2$ with cyclopentylamine (CPA) in the presence of aqueous HCl afforded a layered organic–inorganic hybrid, $[C_5H_9NH_3]_4Cd_3Cl_{10}$ (**1**), containing a two-dimensional $[Cd_3Cl_{10}]^{4-}_n$ network. Herein, we report the crystal structure and the studies of phase transition properties of **1** by variable-temperature single-crystal structure analyses, differential scanning calorimetry (DSC), and dielectric measurements.

EXPERIMENTAL SECTION

Synthesis. Concentrated HCl (4.00 g, 0.04 mol) was added dropwise to cyclopentylamine (1.70 g, 0.02 mol) in water (30 mL). The solution was then added to an aqueous solution of cadmium chloride (3.42 g, 0.015 mol). Large-size colorless block crystals (Figure S1, Supporting Information) of **1** were obtained by slow evaporation of the mixed solution at room temperature after a few weeks. The IR spectra of **1** (Figure S2, Supporting Information) show the N–H stretching vibrations of the RNH_3^+ group at about 3200–3100 cm^{-1}. The RNH_3^+ deformation vibrations are observed at 1591 and 1487 cm^{-1}. The variable-temperature powder X-ray diffraction (PXRD) patterns for **1** are shown in Figure S3 in the Supporting Information. The experimental patterns matching very well with the simulated ones in terms of the crystal structures for the different phases confirms the phase purity of the crystals.

Received: March 11, 2014
Published: August 13, 2014

   dx.doi.org/10.1021/ic500554z | *Inorg. Chem.* 2014, 53, 8913–8918

Crystallography. Variable-temperature X-ray single-crystal diffraction data were collected on a Rigaku Saturn 924 diffractometer with Mo Kα radiation (λ = 0.71073 Å) at 93, 298, and 343 K. Data processing including empirical absorption corrections was performed using the Crystalclear software package (Rigaku, 2005). The structures were solved by direct methods and refined by the full-matrix method based on F^2 by means of the SHELXLTL software package. Non-H atoms were refined anisotropically using all reflections with $I > 2\sigma(I)$. All H atoms were generated geometrically and refined using a "riding" model with $U_{iso} = 1.2U_{eq}$ (C and N). The asymmetric units and the packing views were drawn with DIAMOND (Brandenburg and Putz, 2005). Angles between some atoms were calculated using DIAMOND, and other calculations were carried out using SHELXLTL. Crystallographic data and structure refinement at 93, 298, and 343 K are listed in Table 1.

Table 1. Crystal Data and Structure Refinement for 1 at 93, 298, and 343 K

moiety formula	$4(C_5H_{12}N)$, Cd_3Cl_{10}	$4(C_5H_{12}N)$, Cd_3Cl_{10}	$4(C_5H_{12}N)$, Cd_3Cl_{10}
fw	1036.35	1036.35	1036.35
cryst syst, space group	orthorhombic, $P2_12_12_1$	orthorhombic, *Pbca*	orthorhombic, *Cmca*
temperature (K)	93	298	343
a (Å)	7.4195(14)	19.440(4)	7.584(6)
b (Å)	19.498(4)	7.5603(15)	24.83(2)
c (Å)	24.118(5)	24.644(5)	19.520(13)
volume (Å^3), *Z*	3489.0(12), 4,	3622.0(13), 4,	3676(5), 4
T_{min}/T_{max}	0.408/0.483	0.423/0.496	0.428/0.501
F(000)	2040	2040	2040
reflns collected/ unique	13 245/8019	33 267/4147	12 841/2277
R_{int}	0.0622	0.0545	0.0494
GOF	1.002	1.133	1.118
R_1/wR_2 [$I > 2\sigma(I)$]	0.0375/0.0847	0.0613/0.1621	0.0499/0.1468

DSC Measurement. Differential scanning calorimetry was carried out on a Perkin–Elmer Diamond DSC instrument in the temperature range 170–340 K under nitrogen at atmospheric pressure in aluminum crucibles with a heating rate of 5 K/min.

Dielectric Measurements. The single-crystal samples with silver painted as the electrodes were used for dielectric studies, and the crystal faces selected in the measurements were based on the room-temperature structure. Complex dielectric permittivity ε ($\varepsilon = \varepsilon' - i\varepsilon''$) was measured on a Tonghui TH2828A over the frequency range of 2 kHz to 1 MHz and in the temperature range from 170 to 340 K with the measuring ac voltage fixed at 1 V.

RESULTS AND DISCUSSION

Phase Transitions of 1. The phase transition behavior of **1** was first evidenced by the DSC measurements. Below room temperature, the DSC experiment of **1** shows two reversible heat anomalies at 192.1 and 197.3 K upon the cooling and heating processes, indicating **1** exhibits a reversible phase transition at T_1 = 197.3 K (Figure 1). The wide thermal hysteresis (5.2 K) and the sharp shape of the anomalous peaks reveal the discontinuous character of the transition, indicative of a first-order phase transition. Above room temperature, the DSC result of **1** clearly displays that a reversible phase transition occurs at T_2 = 321.6 K in the heating mode with a narrow thermal hysteresis of 1.6 K (Figure 1). The combined narrow thermal hysteresis and the broad anomalous peaks show that this phase transition is second-order. Entropy changes (ΔS) accompanying the phase transitions at around T_1 and T_2 were estimated to be about 3.712 and 0.751 J/(mol·K),

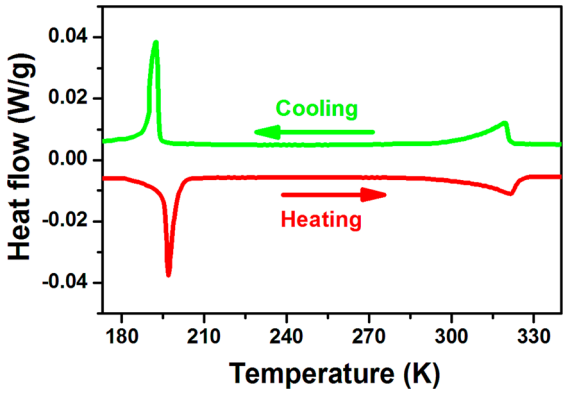

Figure 1. DSC curves of **1**.

respectively. According to the Boltzmann equation, $\Delta S = R \ln(N)$, where R is the gas constant and N is the ratio of the number of respective geometrically distinguishable orientations, the calculated values of $N(T_1)$ and $N(T_2)$ are 1.56 and 1.09, respectively, suggesting the order–disorder feature of the phase transition at T_1 and a complicated phase transition at T_2.[13a,15]

Variable-Temperature Structures of 1. In order to understand the details of these two structural phase transitions, the crystal structures of **1** were determined at 93, 298, and 343 K (Table 1). At 93 K in the low-temperature phase (LTP), **1** crystallizes in the orthorhombic crystal system $P2_12_12_1$ (No. 19). The structure is refined with a racemic twinning model with a Flack parameter[16] of 0.52(3). Upon heating to 298 K in the room-temperature phase (RTP), the crystal structure was solved in the space group *Pbca* (No. 61). When the temperature increases to 343 K in the high-temperature phase (HTP), the space group becomes *Cmca* (No. 64). The relationship between the cells of these three space groups is $-a^{93k} \approx b^{298k} \approx a^{343k}$, $b^{93k} \approx a^{298k} \approx c^{343k}$, and $c^{93k} \approx c^{298k} \approx b^{343k}$. At 93 K, the asymmetric unit of the crystal structure consists of four independent cyclopentylammonium cations (denoted as CPA-A, CPA-B, CPA-C, and CPA-D), three Cd atoms, and 10 Cl atoms (Figure 2a). Each of the three Cd atoms, lying in general positions, is octahedrally coordinated by Cl atoms. The Cd2 atom is coordinated by six bridging Cl atoms, while both the Cd1 and Cd3 atoms are surrounded by one terminal and five bridging Cl atoms. The coordination geometries around the Cd atoms can be described as distorted octahedron, with Cd–Cl distances ranging from 2.495(5) to 2.735(4) Å (Table S1, Supporting Information). These Cd–Cl distances are in good agreement with those found in other structurally similar compounds.[10] The three face-sharing $CdCl_6$ octahedra are connected to their translation-related three face-sharing $CdCl_6$ octahedra by bridging (corner-sharing) Cl atoms, forming a rarely seen two-dimensional network of $[Cd_3Cl_{10}]^{4-}{}_n$ parallel to the *ab* plane (Figures 3a and 4a).[10] The four independent CPA cations locating in the interstitial voids within the network are totally ordered (Figure 3a). Each of the four five-membered rings has an envelope conformation. These CPA cations link the $[Cd_3Cl_{10}]^{4-}{}_n$ network through N–H···Cl hydrogen bonds (Figure 3a). The NH_3 groups of both the CPA-A and CPA-B cations form hydrogen bonds to two bridging (face-sharing) and two terminal Cl atoms with average donor–acceptor distances of 3.309 and 3.336 Å, respectively, while the NH_3 moieties of the CPA-C and CPA-D cations hydrogen bond to four bridging (two face-sharing and two corner-sharing) Cl atoms with average N···Cl distances of 3.412 and 3.332 Å,

dx.doi.org/10.1021/ic500554z | Inorg. Chem. 2014, 53, 8913–8918

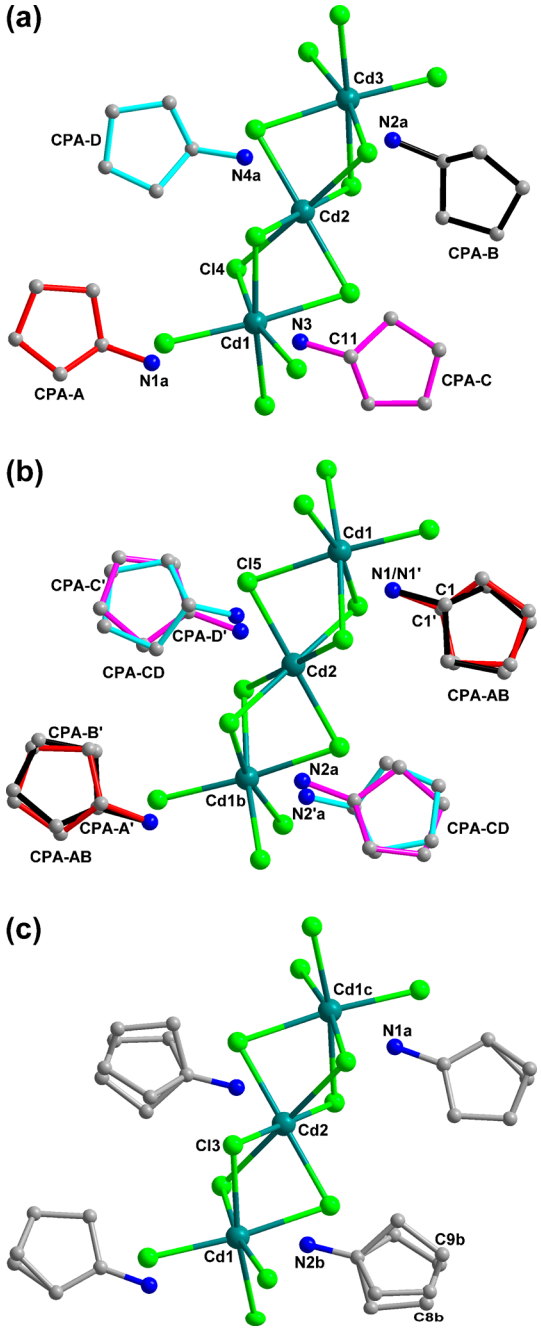

Figure 2. Molecular structures of **1** shown at different temperatures. (a) Low-temperature phase (93 K): the cyclopentylammonium cations are totally ordered. (b) Room-temperature phase (298 K): the cyclopentylammonium cations are orientationally disordered over two positions with 0.5 occupancy. (c) High-temperature phase (343 K): the cyclopentylammonium cations are disordered over two positions about the mirror plane.

respectively (Table S2, Supporting Information). Two layers of CPA cations are embedded between two consecutive inorganic $[Cd_3Cl_{10}]^{4-}{}_n$ layers, forming an alternating organic–inorganic layered structure (Figure 4a).

The basic unit of the crystal structure at 298 K halved the content of that at 93 K, containing two nonequivalent CPA cations (denoted by CPA-AB and CPA-CD) and one-half of the three face-sharing $CdCl_6$ octahedra (Figure 2b). The Cd2 atom lies in a special position on a center of inversion, and accordingly only two independent Cd atoms are present in the

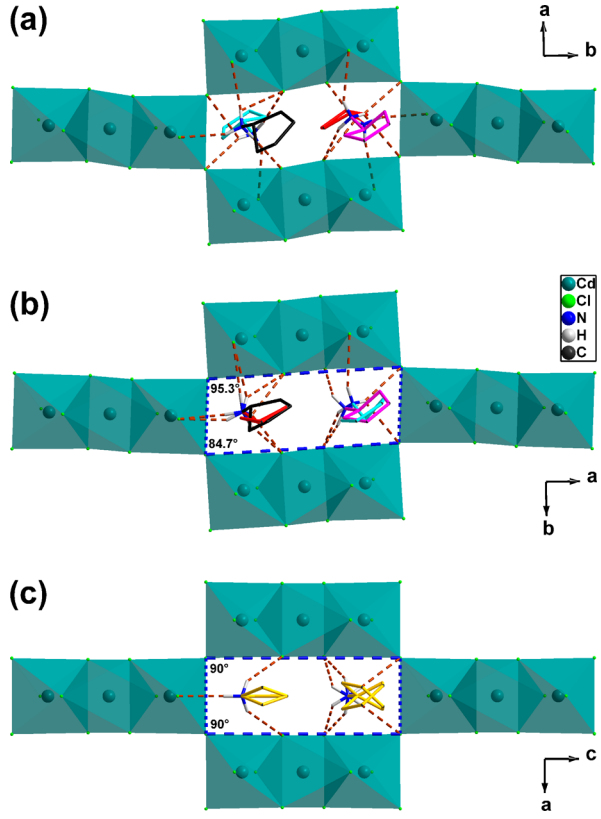

Figure 3. Hydrogen-bonding interactions (brown dashed lines) between the organic and inorganic components in **1** at (a) 93, (b) 298, and (c) 343 K. The blue dashed lines stand for the Cl–Cl edges formed by adjacent corner-sharing Cl atoms in the interstitial void.

three face-sharing $CdCl_6$ octahedra. The Cd–Cl distances (2.495(2)–2.762(2) Å) are similar to those in the LTP (Table S1, Supporting Information). Different from the inorganic layer, the organic layer shows an obvious change in the orientation of the CPA cations. They become highly disordered in the RTP (Figure 2b). The CPA-AB cation is orientationally disordered over CPA-A′ and CPA-B′ positions with 0.5 occupancy, and the CPA-CD cation is also orientationally disordered over two positions, labeling CPA-C′ and CPA-D′, with an occupancy factor of 0.5. The cyclopentyl rings still have envelope conformations. The amine groups of the CPA-A′, CPA-B′, and CPA-D′ cations form hydrogen bonds with the $[Cd_3Cl_{10}]^{4-}{}_n$ network in a manner analogous to those of the CPA-A, CPA-B, and CPA-D cations in the LTP, respectively (Figure 3b). However, the N atom of the CPA-C′ cation acts as a donor to only two face-sharing Cl atoms, different from that of the CPA-C cation in the LTP (Figure 3b). The average N···Cl distances of the N–H···Cl hydrogen bonds involving the N atoms from the CPA-AB and CPA-CD cations are 3.412 and 3.410 Å, respectively, indicating a slight weakening of the hydrogen-bonding interactions (Table S2, Supporting Information). The relatively weaker hydrogen-bonding interactions provide more freedom of the orientational motion of the CPA cations. Except for the disordering of CPA cations, the organic–inorganic layered structure is similar to that in the LTP (Figure 4b).

Compared with those in the RTP, two independent Cd atoms in the HTP are also located in two types of octahedral sites, but the site symmetry changes (Figure 2c). The Cd1 atom, coordinated by one terminal and five bridging Cl atoms,

dx.doi.org/10.1021/ic500554z | Inorg. Chem. 2014, 53, 8913–8918

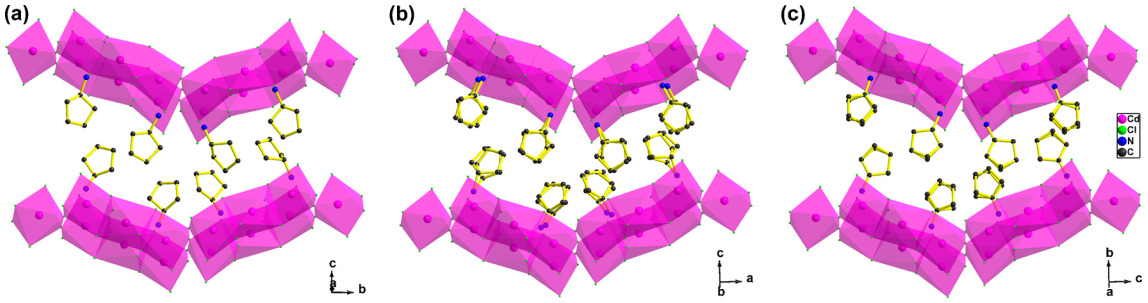

Figure 4. Packing diagrams of **1** at (a) 93, (b) 298, and (c) 343 K. Hydrogen atoms were omitted for clarity.

occupies a special position on the *m* symmetry plane, while the Cd2 atom, surrounded by six bridging Cl atoms, lies in the 2/*m* symmetry site. Both of the nonequivalent CPA cations in the HTP are also orientationally disordered but over two positions about the *bc* plane (Figures 2c and 3c). The conformation of the cyclopentyl rings becoming near planarity as well as the relatively large anisotropic displacement parameters indicates the CPA cations at both positions are still disordered. Hence, the molecular motions of the CPA cations in the HTP become more vigorous. The average N···Cl lengths of the N1a–H···Cl (3.394 Å) and N2b–H···Cl (3.437 Å) hydrogen bonds show no obvious change (Table S2, Supporting Information). Nevertheless, the hydrogen-bonding schemes change, with each H atom from the amine groups having only one acceptor (Figure 3c).

Origins of Phase Transitions of 1. From the above structural analyses, it is clear that the most notable difference between LTP and RTP is the order–disorder transition of the CPA cations. In the RTP, the CPA cations are orientationally disordered over two positions. Below T_1, the orientational motions of the CPA cations are frozen, and each CPA cation has a single orientation. The orientation of the disordered CPA cations during the phase transition process may be along two directions with an equal probability, inducing racemic twinning in the LTP. It appears that the phase transition of **1** at 197.3 K is derived from the order–disorder transition of the CPA cations, which is consistent with the DSC results. A precise analysis of the main packing and structural differences between the RTP and HTP is needed to disclose the phase transition mechanism at 321.6 K. In the HTP, the interstitial void within the network is rectangular with an angle of 90° between the Cl–Cl edges formed by adjacent corner-sharing Cl atoms, while in the RTP, the angles deviate from the right angle value, becoming 95.3° and 84.7°, indicating the distortion of the $[Cd_3Cl_{10}]^{4-}{}_n$ network (Figure 3b,c). Such distortion in **1** is analogous to the change in the tilt system of the octahedra layers in the layered hybrid perovskites, which is one of the origins of the phase transitions of these hybrid perovskites.[7,17] Moreover, the distortion may induce changes in the hydrogen-bonding schemes in the HTP. Therefore, the essential difference between the RTP and HTP is the distortion of the $[Cd_3Cl_{10}]^{4-}{}_n$ network, which is the main driving force of the phase transition of **1** at 321.6 K. The more vigorous molecular motions of the CPA cations in the HTP may also contribute to the phase transition at 321.6 K, which suggests that the mechanism of this phase transition is complicated, corresponding to the DSC analyses.

Dielectric Properties of 1. The temperature-dependent dielectric permittivity of **1** was measured on single-crystal samples along different axes based on the room-temperature structure at selected frequencies. Figure 5 shows the real part (ε') and dielectric loss (tan δ) of the dielectric permittivity

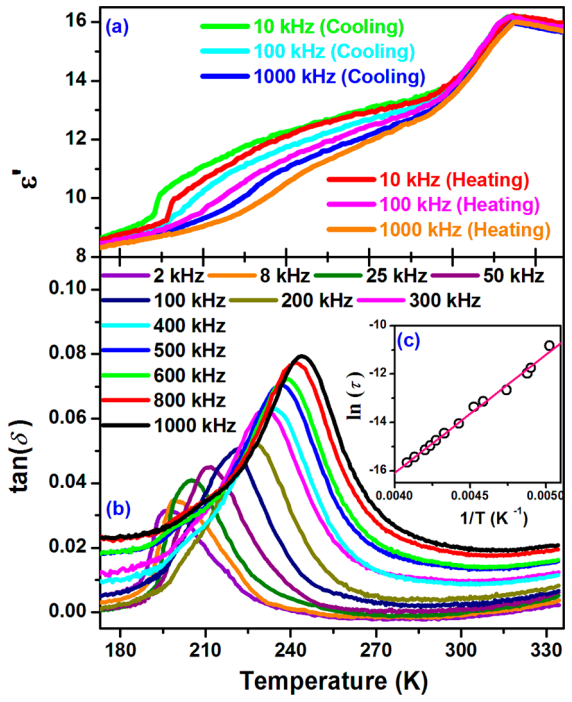

Figure 5. (a) Real part (ε') of the dielectric permittivity of **1** measured along the *b* axis at selected frequencies on heating and cooling; (b) dielectric loss (tan δ) of the dielectric permittivity measured along the *b* axis at selected frequencies on cooling; (c) Arrhenius plots for the dielectric relaxation on cooling.

measured along the *b* axis. Upon heating, the ε' value at 10 kHz increases progressively from 8.6 to a maximal value of 16, accompanied by two step-like anomalies at around T_1 and T_2 (Figure 5a). The changes of the ε' value may be related to the molecular motions of the CPA cations. In the RTP and HTP, the orientationally disordered CPA cations get enough energy to be able to obey the change in the external electric field more easily, which in return enhances their contribution to the polarization, leading to an increase in dielectric permittivity.[18] When the orientational motions of the cations are frozen in the LTP, they possess a weak contribution to the polarization. Two dielectric anomalies also occur during the cooling process, in good accordance with the DSC results. It is interesting to find that the ε' displays a frequency dispersion below room temperature; namely, the temperature where the dielectric anomalies appear moves progressively toward higher temperatures as the frequency increases (Figure 5a). The temperature

dx.doi.org/10.1021/ic500554z | Inorg. Chem. 2014, 53, 8913–8918

of the peak maximum of tan δ also shifts from 195 K at 2 kHz to 245 K at 1000 kHz (Figure 5b). The relaxation behaviors of the dielectric response in **1** could be explained by the peak maxima of tan δ changes obeying the Arrhenius equation $\tau = \tau_0 \exp(E_a/k_BT)$, where τ_0 is the inverse of the frequency factor, E_a denotes the activation energy, k_B denotes the Boltzmann constant, and T is the temperature. For a Debye peak, the equation can be rewritten as $\ln \tau = \ln(2\pi f)^{-1} = \ln(\tau_0) + E_a/k_BT_p$, in which f is the frequency and T_p is temperature of the peak. Thus, E_a and τ_0 can be approximately calculated to be 40.64 kJ/mol and 3.31×10^{-16} s, respectively, according to the experimental data of a $\ln \tau$ versus $1/T$ plot (Figure 5c). Such dielectric relaxation behaviors are also observed in some other compounds that undergo order−disorder type phase transitions.[19] For **1**, the dielectric relaxation behaviors are connected with the order−disorder transition of the cyclopentylammonium cations. As the temperature decreases, the orientational motions of the CPA cations show different responses to the external electric field during the freezing process.

Another remarkable feature of the dielectric properties of **1** is a striking anisotropy along the different crystallographic axes (Figure 6). The values of the real parts at 10 kHz along the *a*

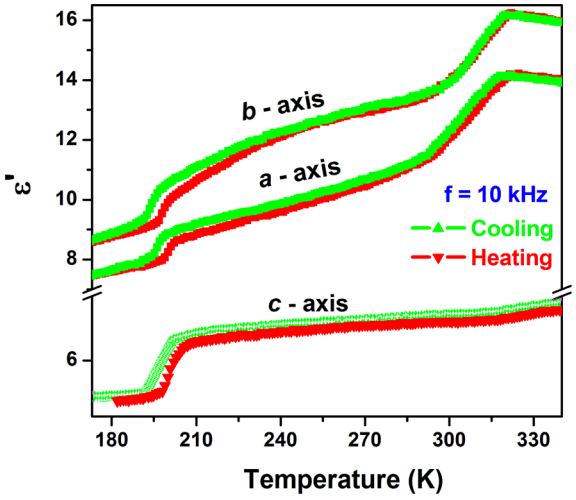

Figure 6. Anisotropic dielectric permittivity (ε') of **1** along the *a*, *b*, and *c* axes at 10 kHz.

and *b* axes are obviously larger than those along the *c* axis. Furthermore, notable anomalies are observed during the phase transition at 321.6 K in the directions of the *a* and *b* axes, while only a very tiny anomaly around 321.6 K is recorded in the direction of the *c* axis. Such a strong dielectric anisotropy can be explained by investigating the intrinsic structural changes in the phase transition processes. The orientationally disordered CPA cations in the RTP will arouse motions along the *a* and *b* axes (Figures 3b and 4b), which yield more dipole-moment components in these two axes. The orientational motions of the CPA cations in the HTP along the *a* and *c* axes (Figures 3c and 4c), corresponding to the *b* and *a* axes in the RTP, respectively, will also make more contribution to the polarization. In addition, the two-dimensional $[Cd_3Cl_{10}]^{4-}{}_n$ network lies in the *ab* plane in the RTP. The shape of the interstitial void within the $[Cd_3Cl_{10}]^{4-}{}_n$ network changes along the *a* and *b* axes during the phase transition at 321.6 K (Figure 3b,c), which also results in the obvious dielectric response in these two axes rather than the *c* axis.

CONCLUSION

In summary, the present work has reported a layered organic−inorganic hybrid complex with two-dimensional $[Cd_3Cl_{10}]^{4-}{}_n$ networks, which exhibits two successive structural phase transitions, at 197.3 and 321.6 K. The combined DSC, variable-temperature structural analyses, and dielectric measurements confirm these two phase transitions and reveal their origins. The phase transition at 197.3 K is induced by the order−disorder transition of the cyclopentylammonium cations, whereas the phase transition at 321.6 K is associated with the distortion of the $[Cd_3Cl_{10}]^{4-}{}_n$ network.

ASSOCIATED CONTENT

Supporting Information

Crystal picture, variable-temperature PXRD patterns, and IR spectrum. Selected Cd−Cl distances and hydrogen bond geometry of the crystal structures. CCDC reference numbers: 987766 (LT (93 K)), 987767 (RT (298 K)), and 987768 (HT (343 K)). This material is available free of charge via the Internet http://pubs.acs.org.

AUTHOR INFORMATION

Corresponding Authors

*(G.-Q. Mei) E-mail: yc_mgq@163.com.
*(Y. Zhang) E-mail: yizhang1980@seu.edu.cn.

Notes

The authors declare no competing financial interest.

ACKNOWLEDGMENTS

This work was supported by the National Natural Science Foundation of China (Grants 21371032, 21101025, and 21261024). Also we gratefully thank Prof. Ren-Gen Xiong for revising the manuscript.

REFERENCES

(1) (a) Wuttig, M.; Yamada, N. *Nat. Mater.* **2007**, *6*, 824−832. (b) Salinga, M.; Wuttig, M. *Science* **2011**, *332*, 543−544. (c) Lencer, D.; Salinga, M.; Wuttig, M. *Adv. Mater.* **2011**, *23*, 2030−2058. (d) Zheng, H.; Rivest, J. B.; Miller, T. A.; Sadtler, B.; Lindenberg, A.; Toney, M. F.; Wang, L. W.; Kisielowski, C.; Alivisatos, A. P. *Science* **2011**, *333*, 206−209.

(2) (a) Sun, Z. H.; Luo, J. H.; Zhang, S. Q.; Ji, C. M.; Zhou, L.; Li, S. H.; Deng, F.; Hong, M. C. *Adv. Mater.* **2013**, *25*, 4159−4163. (b) Mączka, M.; Pietraszko, A.; Macalik, B.; Hermanowicz, K. *Inorg. Chem.* **2014**, *53*, 787−794. (c) Sun, Z. H.; Luo, J. H.; Chen, T. L.; Li, L. N.; Xiong, R.-G.; Tong, M. L.; Hong, M. C. *Adv. Funct. Mater.* **2012**, *22*, 4855−4861. (d) Mączka, M.; Gągor, A.; Macalik, B.; Pikul, A.; Ptak, M.; Hanuza, J. *Inorg. Chem.* **2014**, *53*, 457−467.

(3) (a) Mitzi, D. B. *J. Chem. Soc., Dalton Trans.* **2001**, 1−12. (b) Huang, S. D.; Shan, Y. *J. Solid State Chem.* **2000**, *152*, 229−235. (c) Huang, T.; Vanchura, B. A.; Shan, Y. K.; Huang, S. D. *J. Solid State Chem.* **2007**, *180*, 2110−2115.

(4) (a) Kagan, C. R.; Mitzi, D. B.; Dimitrakopoulos, C. D. *Science* **1999**, *286*, 945−947. (b) Xu, G. C.; Ma, X. M.; Zhang, L.; Wang, Z. M.; Gao, S. *J. Am. Chem. Soc.* **2010**, *132*, 9588−9590. (c) Xu, G. C.; Zhang, W.; Ma, X. M.; Chen, Y. H.; Zhang, L.; Cai, H. L.; Wang, Z. M.; Xiong, R.-G.; Gao, S. *J. Am. Chem. Soc.* **2011**, *133*, 14948−14951. (d) Liu, B.; Shang, R.; Hu, K. Li.; Wang, Z. M.; Gao, S. *Inorg. Chem.* **2012**, *51*, 13363−13372.

(5) (a) Polyakov, A. O.; Arkenbout, A. H.; Baas, J.; Blake, G. R.; Meetsma, A.; Caretta, A.; van Loosdrecht, P. H. M.; Palstra, T. T. M.

Chem. Mater. **2012**, *24*, 133−139. (b) Vishwakarma, A. K.; Ghalsasi, P. S.; Navamoney, A.; Lan, Y.; Powell, A. K. *Polyhedron* **2011**, *30*, 1565−1570. (c) Naik, V. V.; Vasudevan, S. *J. Phys. Chem. C* **2010**, *114*, 4536−4543. (d) Mercier, N.; Poiroux, S.; Riou, A.; Batail, P. *Inorg. Chem.* **2004**, *43*, 8361−8366. (e) Billing, D. G.; Lemmerer, A. *Acta Crystallogr., Sect. B: Struct. Sci.* **2007**, *63*, 735−747.
(6) Mitzi, D. B. *Prog. Inorg. Chem.* **1999**, *48*, 1−121.
(7) Depmeier, W. *Acta Crystallogr., Sect. B: Struct. Sci.* **1977**, *33*, 3713−3718.
(8) (a) Zouari, F.; Salah, A. B.; Daoud, A. *Phase Transitions* **1999**, *70*, 1−9. (b) Chapuis, G.; Arend, H.; Kind, R. *Phys. Status Solidi A* **1975**, *31*, 449−454. (c) Heger, G.; Mullen, D.; Knorr, K. *Phys. Status Solidi A* **1976**, *35*, 627−637.
(9) (a) Doudin, B.; Chapuis, G. *Acta Crystallogr., Sect. B: Struct. Sci.* **1990**, *46*, 175−180. (b) Chapuis, G. *Acta Crystallogr., Sect. B: Struct. Sci.* **1978**, *34*, 1506−1512.
(10) Gagor, A.; Waśkowska, A.; Czapla, Z.; Dacko, S. *Acta Crystallogr., Sect. B: Struct. Sci.* **2011**, *67*, 122−129.
(11) Fu, D. W.; Cai, H. L.; Liu, Y. M.; Ye, Q.; Zhang, W.; Zhang, Y.; Chen, X. Y.; Giovannetti, G.; Capone, M.; Li, J. Y.; Xiong, R.-G. *Science* **2013**, *339*, 425−428.
(12) (a) Zhang, Y.; Zhang, W.; Li, S. H.; Ye, Q.; Cai, H. L.; Deng, F.; Xiong, R.-G.; Huang, S. D. *J. Am. Chem. Soc.* **2012**, *134*, 11044−11049. (b) Ye, Q.; Akutagawa, T.; Endo, T.; Noro, S.; Nakamura, T.; Xiong, R.-G. *Inorg. Chem.* **2010**, *49*, 8591−8600. (c) Ye, Q.; Akutagawa, T.; Hoshino, N.; Kikuchi, T.; Noro, S.; Xiong, R.-G.; Nakamura, T. *Cryst. Growth Des.* **2011**, *11*, 4175−4182.
(13) (a) Zhang, Y.; Ye, H. Y.; Fu, D. W.; Xiong, R.-G. *Angew. Chem., Int. Ed.* **2014**, *53*, 2114−2118. (b) Zhang, W.; Ye, H. Y.; Cai, H. L.; Ge, J. Z.; Xiong, R.-G.; Huang, S. D. *J. Am. Chem. Soc.* **2010**, *132*, 7300−7302.
(14) (a) Zhang, Y.; Ye, H. Y.; Zhang, W.; Xiong, R.-G. *Inorg. Chem. Front.* **2014**, *1*, 118−123. (b) Zhang, Y.; Awaga, K.; Yoshikawa, H.; Xiong, R.-G. *J. Mater. Chem.* **2012**, *22*, 9841−9845. (c) Zhang, Y.; Liao, W. Q.; Ye, H. Y.; Fu, D. W.; Xiong, R.-G. *Cryst. Growth Des.* **2013**, *13*, 4025−4030.
(15) (a) Jain, P.; Ramachandran, V.; Clark, R. J.; Zhou, H. D.; Toby, B. H.; Dalal, N. S.; Kroto, H. W.; Cheetham, A. K. *J. Am. Chem. Soc.* **2009**, *131*, 13625−13627. (b) Li, S. G.; Luo, J. H.; Sun, Z. H.; Zhang, S. Q.; Li, L. N.; Shi, X. J.; Hong, M. C. *Cryst. Growth Des.* **2013**, *13*, 2675−2679. (c) Szklarz, P.; Owczarek, M.; Bator, G.; Lis, T.; Gatner, K.; Jakubas, R. *J. Mol. Struct.* **2009**, *929*, 48−57.
(16) Flack, H. D. *Acta Crystallogr.* **1983**, *A39*, 876−881.
(17) Depmeier, W.; Felsche, J.; Wildermuth, G. *J. Solid State Chem.* **1977**, *21*, 57−65.
(18) Hajlaoui, S.; Chaabane, I.; Oueslati, A.; Guidara, K. *Solid State Sci.* **2013**, *25*, 134−142.
(19) (a) Fu, D. W.; Zhang, W.; Cai, H. L.; Zhang, Y.; Ge, J. Z.; Xiong, R.-G.; Huang, S. D. *J. Am. Chem. Soc.* **2011**, *133*, 12780−12786. (b) Fu, D. W.; Zhang, W.; Cai, H. L.; Zhang, Y.; Ge, J. Z.; Xiong, R.-G.; Huang, S. D.; Nakamura, T. *Angew. Chem., Int. Ed.* **2011**, *50*, 11947−11951.